Similarities in ground- and satellite-based NDVI time series and their relationship to physiological activity of a Scots pine forest in Finland

Quan Wang[a,*], John Tenhunen[a], Nguyen Quoc Dinh[a], Markus Reichstein[a],
Timo Vesala[b], Petri Keronen[b]

[a]Department of Plant Ecology, University of Bayreuth, Bayreuth D-95440, Germany
[b]Department of Physical Sciences, University of Helsinki, 00014 Helsinki, Finland

Abstract

Daily time-step normalized difference vegetation index (NDVI) time series from satellite-derived (NOAA/AVHRR, SPOT/VEGETATION, TERRA/MODIS) and ground-based micrometeorological sensors were evaluated for a coniferous pine forest (*Pinus sylvestris* L.) located in Hyytiälä, Finland. Micrometeorology-based broadband NDVI was calculated from observed upward and downward photosynthetically activity radiation (PAR) and global radiation measurements. The composite satellite-derived NDVI time series were smoothed with a best index slope extraction method (BISE) and adjusted Fourier transform (AFT) in order to downscale from the compositing period to daily scale.

The broadband and satellite-derived NDVIs were highly correlated during the main growth period (Julian days 90–270), but poorly correlated when the entire year was considered, i.e., large differences occurred during winter. High correlations were also found between the seasonal courses for broadband NDVI and daily air temperature. The analysis revealed that the onset of greenness in spring was consistently determined from broadband NDVI time series in different years, but that fluctuations in NDVI during the late season transition to winter dormancy prevented reliable prediction of the termination in physiological activity. Efforts to retrieve the same relationships during spring from satellite-derived NDVI failed.

After comparing the smoothed time series from different NDVI determinations, we examined the relationship between NDVI, gross primary production (GPP) and FAPAR. An obvious exponential relationship is found between broadband NDVI and GPP (R^2=0.72 for clear weather conditions; also detectable from the satellite sensors), while a linear relationship occurs between broadband NDVI and FAPAR (R^2=0.79). FAPAR in relation to satellite-derived NDVI is best described with a logistic curve under clear weather conditions, but the level of correspondence is low (R^2=0.53). Overall, broadband NDVI is a good index to describe physiological activity of the pine forest during certain periods, i.e. provides a means for obtaining other physiological parameters that are required by ecosystem models. However, during the late season, broadband NDVI estimated over the pine stand is influenced by more than vegetation physiological activity. Though satellite-derived NDVI is more difficult to link to GPP, it may still provide useful information under clear weather conditions. Satellite-derived NDVI remains our only choice for generalization in large-scale investigations. Thus, intensified examination of the influences of smoothing and downscaling of satellite-derived NDVI is inevitable.
© 2004 Elsevier Inc. All rights reserved.

Keywords: NDVI time series; Broadband NDVI; Micrometeorology; Scots pine forest; GPP; FAPAR

1. Introduction

The normalized difference vegetation index (NDVI) is one of most commonly used vegetation indices for land cover classification (Brown et al., 1993; Evans et al., 1993; Loveland et al., 1991; Townshend et al., 1994), derivation of

---

vegetation biophysical properties (Asrar et al., 1992; Goward & Huemmrich, 1992; Sellers et al., 1994), estimation of net primary production (Prince, 1991; Running and Nemani, 1988; Tucker & Sellers, 1986), and monitoring of environmental impacts (cf. Wang et al., 2003). A wide variety of analytical methods have been developed from NDVI time series data to (1) establish seasonal and interannual trends in vegetation properties such as phenological change (e.g., Duchemin et al., 1999; Hill & Donald, 2003; Moody & Johnson, 2001; Reed et al., 1994) and (2) derive biophysical parameter values for physically based models of climate, hydrology, net primary production, and biogeochemical cycling (Goward et al., 1987, 1985; Liu et al., 1999; Prince & Tucker, 1986; Running & Hunt, 1993; Sellers et al., 1994; Spanner et al., 1990; Tucker & Sellers, 1986). Temporal sequence data from satellite observations have been used to characterize the timing, dynamics, and distribution of phytophenological events (Azzali & Menenti, 1999), observations that are critical for quantification of ecosystem carbon balances and carbon sequestration by the biosphere.

NDVI time series are commonly obtained from the advanced very high resolution radiometer (AVHRR) GAC data source (James & Kalluri, 1994) and 1-km data source (Eidenshink & Faundeen, 1994), from the SPOT4-VEGE-TATION data source (Duchemin & Maisongrande, 2002), and the MODIS data source (Van Leeuwen et al., 1999). Compositing methods have been developed to remove environmental influences, such as cloud cover, and to improve the stability of NDVI time series data (e.g., Holben, 1986; Van Leeuwen et al., 1999; Duchemin et al., 2002). By compositing, temporal resolution is lost, making it difficult to compare directly with land surface observations (Huemmrich et al., 1999). One way to again increase temporal resolution to a daily time-step is to interpolate from a function fit to a smoothed NDVI time series. However, the interpolation can introduce large biases. To our knowledge, few studies have reported on the accuracy of smoothed NDVI time series, seemingly due to the lack of appropriate ground-based NDVI data.

As an alternative to satellite or ground-based spectror-adiometer derived NDVI, Huemmrich et al. (1999) calcu-lated broadband NDVI time series from tower-mounted photosynthetically active radiation (PAR) and global radi-ation (both incoming and reflected above the canopies) sensors at four Boreal Ecosystem–Atmosphere Study (BOREAS) sites. The comparisons between broadband and narrow-band nadir-viewed NDVI indicated good agree-ment. The advantage of broadband NDVI over satellite-derived NDVI time series is that temporal resolution at a daily time-step or higher is achieved, without the influences of angular geometry and essentially without atmospheric disturbances. We report here 5 years of daily broadband NDVI observations (according to the method of Huemmrich et al., 1999) obtained over a Scots pine forest in Hyytiälä, Finland. Since for large-scale applications, satellite-derived

NDVI time series data remain essential, understanding of smoothed and interpolated information from composited NDVI observations is critical for the construction of models. The definition of appropriate smoothing methods may directly decide the success of applications, if composited data may be used at all. Thus, an objective of the paper is to compare the satellite-derived NDVI time series after smoothing with the broadband NDVI time series at the Hyytiälä tower site. Both broadband and satellite-borne NDVI time series are tested for their usefulness in describing phenological changes in the pine forest as captured by seasonal courses in radiation absorption of the canopy (FAPAR) and estimated gross primary production (GPP).

2. Materials and methods

2.1. Hyytiälä pine forest site and radiation observations

Ground-based measurements were carried out at the Station for Measuring Forest Ecosystems–Atmosphere Relation (SMEAR II) in Hyytiälä forestry field station located in Finland (61°51′ N, 24°17′ E). It is one of 15 sites within the network of the EUROFLUX ('long-term carbon dioxide and water vapor fluxes of European forests and interactions with the climate system') (Tenhunen et al., 1998; Valentini, 2003). Scots pine (Pinus sylvestris L.) dominates the vegetation with only 1% of the canopy made up of other species within ca. 200 m of the tower. The homogeneous fetch reaches ca. 1200 m. The stand was planted in 1962 and the mean height of the trees reached 12 m with the average breast height diameter (BHD) of 13 cm in 1996. The stem density is ca. 2500 stems ha^{-1} with total biomass of 45 t ha^{-1}. And the projected leaf area index of this tree stand is 3. The understory consists of a well-developed canopy of Vaccinium myrtillus, which may play an important role in ecosystem function at this site. The soil can be characterized as a sandy to coarse silty glacial till.

A 73-m high mast and a 15-m tower are used to measure meteorological parameters and gas composition as well as the gas exchange of the trees, cf. Vesala et al. (1998). Incoming global radiation and PAR are measured at 18 m height, while reflected global radiation and PAR are measured at 70 m height. The radiation sensors for global radiation (both incoming and reflected) are the Reemann TP 3 pyranometer (Astrodata, Tartu, Estonia) and for PAR the LI-190SZ quantum sensor (LiCor, Lincoln, NE, USA). The wavelength range of the pyranometer is from 0.3 to 4.8 μm, while PAR sensors include from 0.4 to 0.7 μm. Hourly time-step data were retrieved by averaging the output for 60-min intervals. For the conversion of photon flux density (μmol m^{-2} s^{-1}) to energy flux density (W m^{-2}), conversion factors from Ross and Sulev (2000) have been applied in the paper (0.2195 for incoming PAR and 0.2072 for reflected PAR).

2.2. Broadband NDVI and FAPAR for Hyytiälä

The definition of NDVI utilizes differences in leaf absorptance in the red and near-infrared regions (Deering, 1978):

$$NDVI = \frac{X_{NIR} - X_R}{X_{NIR} + X_R} \tag{1}$$

where X can be digital counts, at-satellite radiance, top of the atmosphere apparent reflectances, land-leaving surface radiance, surface reflectances, or hemispherical spectral albedos (Huete et al., 1999).

Huemmrich et al. (1999) replaced the red domain with PAR and the near-infrared with an optical infrared domain in order to use the upward and downward PAR and global radiation sensors measurements. Thus, the broadband NDVI is calculated from:

$$NDVI_b = \frac{\rho_{OIR} - \rho_{PAR}}{\rho_{OIR} + \rho_{PAR}} \tag{2}$$

where ρ_{PAR} is PAR reflectance (the ratio of reflected and incoming PAR measured by downward and upward PAR sensors),

$$\rho_{PAR} = \frac{PAR_{refl}}{PAR_{in}} \tag{3}$$

and ρ_{OIR} is the reflectance of optical infrared radiance (irradiance value between the difference of global radiation and PAR), thus ρ_{OIR} is calculated from:

$$\rho_{OIR} = \frac{GR_{refl} - PAR_{refl}}{GR_{in} - PAR_{in}} \tag{4}$$

where GR_{in} and GR_{refl} are incoming and reflected global radiation, respectively.

Relationships between vegetation indexes with fraction of absorbed photosynthetically active radiation have been established both theoretically (Choudhury, 1987; Knyazi-khin et al., 1999; Sellers, 1987) or empirically (Gamon et al., 1995; Wylie et al., 2002). These studies relate mainly to satellite-derived NDVI, but similar approaches may be taken with respect to broadband NDVI. In this case,

$$FAPAR = \frac{PAR_{in} - PAR_{refl}}{PAR_{in}} \tag{5}$$

This calculation neglects the PAR penetrating through the canopy and absorbed by the ground. However, the small percentage of ground absorbed PAR has little effect on the analysis.

2.3. Satellite-derived NDVI for Hyytiälä

NOAA AVHRR weekly NDVI data from 1996 through 1998 and the year 2000 were obtained from the German Remote Sensing Data Center (DFD). This weekly product is based on NOAA-14 AVHRR data and maximum value compositing over 21 AVHRR passes during the period.

Before compositing, special emphasis has been given to a precise image registration and a cloud screening procedure to ensure that only cloud free pixels are taken for the latter compositing process. This is based on a mixture of unsupervised pre-processing steps and a supervised parameterization of the cloud tests and an image navigation control. The 1998 through 2001 SPOT VEGETATION NDVI (first version) on a 10-day basis were downloaded from the free VEGETATION products site (http://www.free.vgt.vito.be/), and 2001 TERRA MODIS NDVI and EVI (version 3) were obtained from the Earth Observing System Data Gateway on a 16-day basis (EOS, http://edcimswww.cr.usgs.gov/pub/imswelcome/). All the products have a spatial resolution of 1 km. And the data from the tower site pixel were extracted.

Several factors other than land surface characteristics influence the stability of the satellite-derived NDVI, e.g., cloud contamination, atmospheric variability, and bidirectional reflectance (Gutman, 1991). The changes in NDVI caused by these factors are seen as undesirable noise in vegetation studies. Thus, compositing methods have been developed to eliminate these effects. The currently accepted procedure is the maximum value composite technique (MVC, Holben, 1986), which has been applied to the AVHRR NDVI data source. The MVC selects the maximum NDVI value on a per-pixel basis over a set compositing period. It performs better over near-Lambertian surfaces and for data uncorrected for atmospheric composition (Cihlar et al., 1994), which is not suitable for MODIS (atmospheric corrected according to Van Leeuwen et al., 1999). The MODIS algorithm selects all reflectance data from a 16-day period, based on data integrity and cloud flags, and fits the Walthall BRDF model to the individual band data before the final calculation of NDVI. The first version of SPOT-VEGETATION data is derived using the MVC method, but a new method designated as bidirectional compositing (BDC) has been designed to allow anisotropy removal by retrieving BRDF (Duchemin et al., 2002; Duchemin & Maisongrande, 2002).

Considerable noise remains in satellite-derived NDVI time series data even after application of the various compositing methods. Missing data or periods where the stored values are obtained under cloudy conditions often lead to sudden and large decreases in NDVI. One approach to deal with this problem is to smooth NDVI profiles using statistical filters (e.g., Dijk et al., 1987), but statistical filters generally do not remove noise. Sellers et al. (1994) applied Fourier wave adjustment of outliers in the NDVI time series to eliminate large and sudden decreases. Viovy et al. (1992) proposed the best index slope extraction (BISE) as an alternative to MVC method to reduce noise in NDVI time series.

The satellite-derived NDVI data used here is the composite data available from the above listed data sources, not originally recorded data. Our goal is to post-process these data such that stability is improved (eliminating the

remaining effects from clouds which occur over long periods) and smooth temporal trends that allow estimation of NDVI on a daily basis for comparison with ground-based measurements are identified. Examination of the results from post-processing of the data products seems appropriate, since these data provide the starting point in most applications and the problems are continually confronted. Two different smoothing methods that were designed for compositing NDVI time series have been further used were used here in post-processing steps, namely BISE and Fourier wave adjustment.

2.3.1. BISE

Originally, BISE was designed as an alternative to MVC and was applied to daily NDVI data (Viovy et al., 1992). The BISE algorithm assumes (1) that clouds and other factors will only decrease NDVI values, (2) data transmission errors will cause abnormally high NDVI, and (3) that actual vegetation-related NDVI decreases (e.g., due to cutting of meadows, removal of trees, etc.) may be sudden but will persist for relatively long time periods since any vegetation re-growth is relatively slow. Considering composite data, assumption (2) is no longer needed. Based on these assumptions, we accept only large decreases in NDVI when there are no values in the subsequent 30 days that are greater than 120% of the immediate low value. Subsequent large increases are assumed to occur due to the ending of cloudy periods. The threshold of 20% is same as used by Viovy et al. (1992), while the 'sliding period' of 30 days for considering whether an actual change in vegetation has occurred is based on our experience with the frequency of cloudiness in Western Europe. Thus, for AVHRR, the next three NDVI data in time series are taken into account, next two for SPOT-VEGETATION, and next one for MODIS NDVI data.

2.3.2. Adjusted Fourier transformation (AFT)

Decomposition of temporal data to the frequency domain can be achieved using Fourier analysis, in which frequency information is represented as constituent sine and cosine functions (Briggs & Hensen, 1995). Decomposed signals can be converted back to the temporal domain through the inverse Fourier transform. If the original data is discrete rather than continuous, the discrete Fourier transform (DFT) which requires a regular spacing of samples within the temporal domain should be applied. Fourier analysis is an objective, consistent, and concise summarization of the temporal signature that is sensitive to systematic changes in vegetation and applied widely in NDVI phenology analysis (e.g., Azzali & Menenti, 1999; Moody & Johnson, 2001; Sellers et al., 1994).

The discrete Fourier transform is given by

$$y_k = \frac{1}{N} \sum_{k=0}^{N-1} c_k e^{-i2\pi k/N} \qquad (6)$$

where N is the number of samples in the time series, k is the current sample number, i is an imaginary number, and c is the kth sample value.

Substituting Euler's equation into the DFT formula and expanding gives:

$$y_n = a_0 + a_1 \cos\left(\frac{2\pi n}{N} + b_1\right) \sin\left(\frac{2\pi n}{N}\right) + a_2 \cos\left(\frac{4\pi n}{N}\right)$$
$$+ b_2 \sin\left(\frac{4\pi n}{N}\right) + \ldots + a_k \cos\left(\frac{2k\pi n}{N}\right) + b_k \sin\left(\frac{2k\pi n}{N}\right) \qquad (7)$$

where a_0 is the mean, a_1 and b_1 are first-order trigonometrics, a_2 and b_2 are second-order trigonometrics, and so on to the kth order. Each order represents a harmonic.

The composite NDVI time series are obtained with a composite period sampling rate, which fits to the requirement of DFT. Although several harmonics can be produced from DFT, only the first two harmonics are included in inverse transformation. The determination of trigonometric coefficients is based on the modification of Sellers et al. (1994), which applies robust least-squares optimizing (taking into account that errors in NDVI result in lower values; AFT). Thus, negative deviations receive low weights and positive deviations high weights during fitting. The detailed procedures are given in Appendix A.

2.4. GPP determinations at the Hyytiälä site

The GPP dataset in Hyytiälä site was obtained from tower eddy covariance measurements and micrometeorological data following the methods described by Falge et al. (2003). A detailed description of steps in the procedure is given in Wang et al. (2004). In summary, continuous measurements of NEE and microclimate parameters at a half-hourly time step from 1997 to 2000 were gap filled (Falge et al., 2001, look-up table method) and were used to extract estimates of half-hourly step GPP and ecosystem respiration (R_{eco}). GPP is obtained by adding R_{eco} to the observed net ecosystem exchange (NEE) by the eddy covariance technique. R_{eco} may be estimated from the observations via several methodologies (Falge et al., 2002). Only R_{eco} estimated from nighttime data was applied here, where:

$$R_{eco} = R_{eco-Tref} e^{\left(\frac{E_a}{R}\left(\frac{1}{T_{ref}} - \frac{1}{T_K}\right)\right)} \qquad (8)$$

$R_{eco-Tref}$ (the ecosystem respiration rate at reference temperature, T_{ref}, of 283.16 K) and E_a, the activation energy in J mol^{-1}, are fitted site-specific parameters, R is the gas constant (8.134 J K^{-1} mol^{-1}), and T_K the soil temperature at a depth of 5 cm or the air temperature measured above the canopy. In the analysis conducted here, we used the air temperature above the canopy.

The regression was first fit to nighttime data for the entire year to obtain an estimate of E_a applicable over a broad

range in nighttime temperature. Subsequently, E_a was held constant and $R_{eco-Tref}$ fit for 21-day periods for each data set starting on January 1 of each year. The parameters were then used to estimate temperature dependent corrections on a half-hour basis at the temperatures observed during the daytime period, i.e., to obtain half-hourly GPP. Hourly step GPP dataset was obtained through averaging the two half-hourly GPP values for each hour. Daily GPP was estimated by integrating all half-hour GPP within the time from sunrise to sunset on each day.

3. Results

3.1. Broadband NDVI

3.1.1. Relationship to phenology

Broadband NDVI was calculated from measurements of PAR and global radiation over the canopy on a daily basis for 1997–2001 except the year 1998 when a global radiation sensor failed to function. In order to remove possible errors in further analysis when comparing with satellite-derived NDVI, the measurements were evaluated at the approximate time of satellite overpasses. These were 10:00 LT for VEGETATION and MODIS and 14:00 LT for AVHRR. Thus, two broadband NDVI time series were obtained that corresponded to these two times of day.

Fig. 1 shows the broadband NDVI in various years at daily time-step (only the 14:00 LT time series is presented). Spikes are observed in the curves when including all days. These consistently occur between Julian days (JD) 1 and 60 or after JD 270. Clear days occur in Hyytiälä mainly within the growing season, while winter has long periods with continuous cover by clouds. Selecting only clear day points as Huemmrich et al. (1999), re-occurring trends in NDVI over the season are clearly seen within the period JD 80–250. Smoothing the overall data with a moving mean provides a longer time sequence but includes inherent noise. Interpretation of this smoothed NDVI remains difficult during the winter period indicated.

Ignoring the winter period with noisy data (probably due to changes in snow cover and reflectance changes associated with cloudy weather), a broadband NDVI value of ca. 0.5 was consistently observed with increase in clear days in spring (ca. JD 90–100). NDVI then increased to a maximum value of ca. 0.75–0.8 throughout summer, followed by a slow decrease between JD 230 and 270 (recognizable only during 1999 and 2000 with a longer period in late season with clear days).

Reed et al. (1994) suggested criteria to link NDVI changes to vegetation phenology. According to their methods, phenological change is indicated where momentary data correspond to the moving mean and where an increasing or decreasing trend is observed. Onset of greenness occurs where the maximum sustained number of days are found with increasing NDVI, while the end-of-season
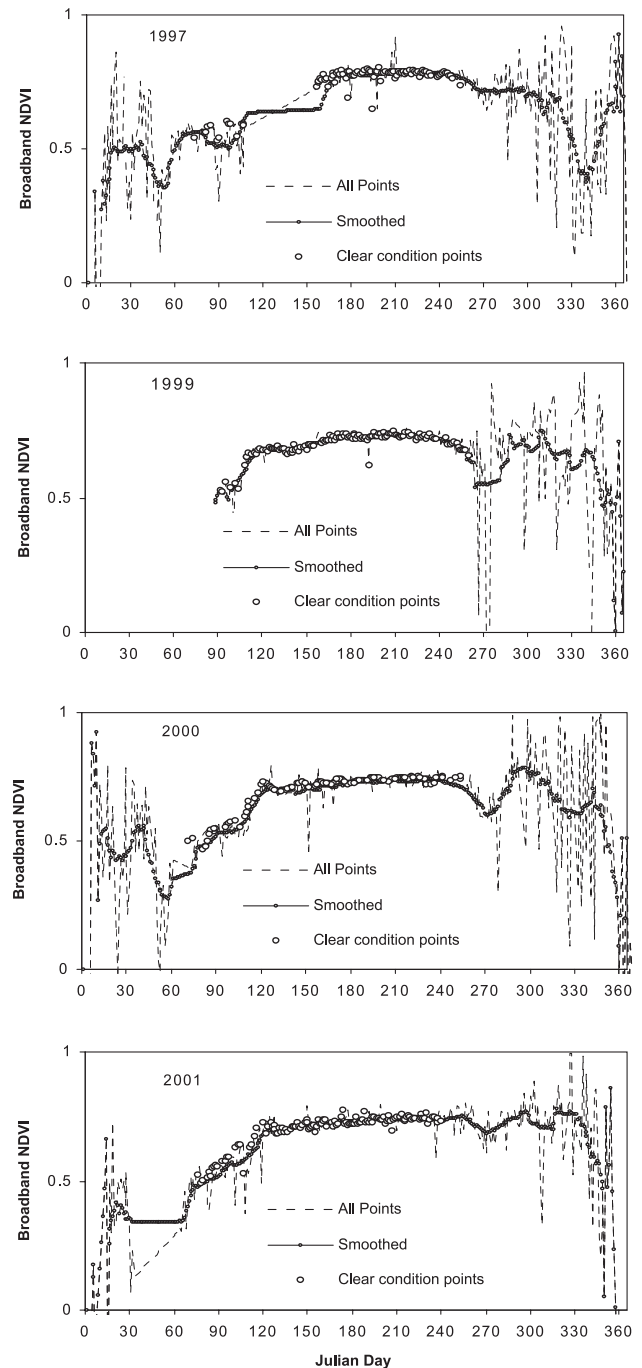

Fig. 1. Daily broadband NDVI in Hyytiälä site, Finland for 1997, 1999, 2000, and 2001. NDVI time series are based on 14:00 LT observations.

may be determined from a similar decreasing NDVI trend. As pointed out by Reed et al. (1994), the selection of the averaging period influences the final result, since a long time interval results in a less sensitive trend detector and a short interval is responsive to insignificant trend changes. For the Hyytiälä data, a period of 15 days was found to provide correspondence between the moving mean and individual observations.

According to such phenological criteria (cf. Reed et al., 1994), the beginning of the growing season is recognizable

where NDVI consistently takes on a value of ca. 0.52–0.54 and then begins to increase. However, the end-of-season is not definable from the NDVI time series, since large variation in NDVI are observed after JD 270. The maximum NDVIs occur late in the growing season. Variations in NDVI after JD 270 seem most easily explained as controlled by abiotic factors, since strong winter hardening is to be expected at the Hyttiälä site.

3.1.2. Relationship with air temperature

As seen in Fig. 2, broadband NDVI and daily average air temperature exhibit similar annual patterns. NDVI increases when air temperature surpasses 0 °C and tend to increase until the temperature is over 10 °C. Cross correlation (Fig. 3) demonstrated that there was no time
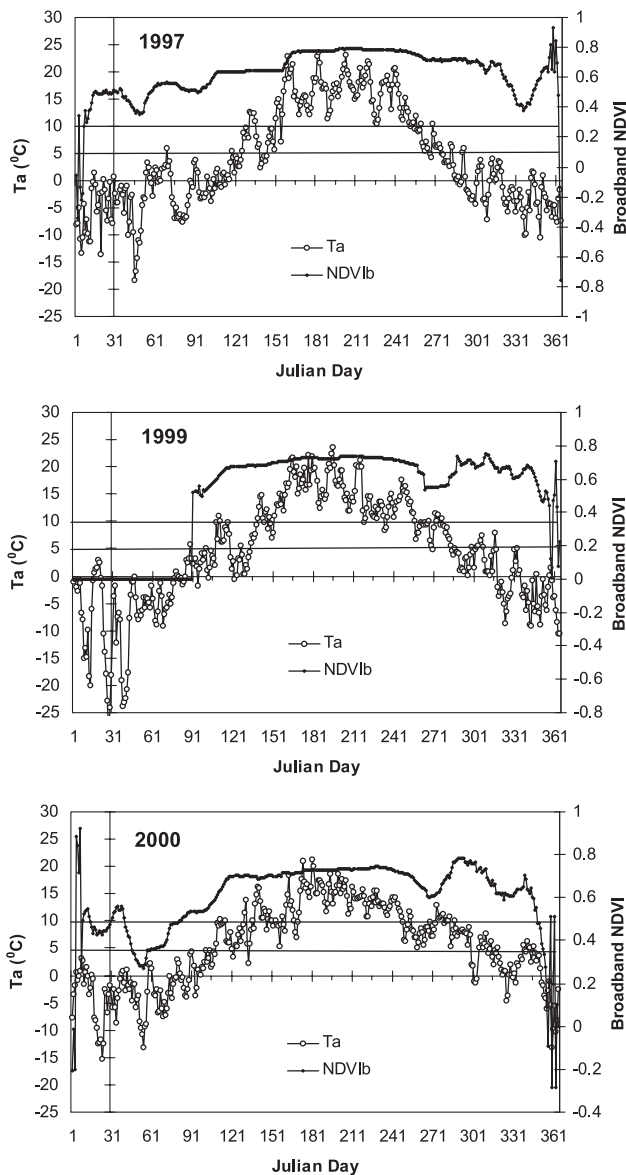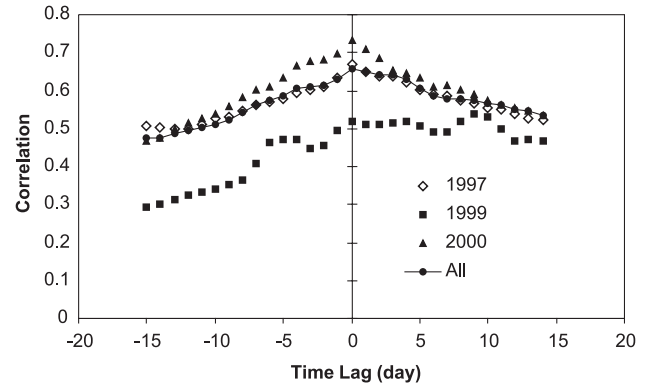

Fig. 3. Cross correlation between broadband NDVI and air temperature with different time lags at Hyytiäla site, Finland in 1997, 1999, and 2000.

lag between broadband NDVI and daily average air temperature. The correlation coefficient was lower in 1999 at 0.52, compared with 0.67 and 0.73 in year 1997 and 2000, respectively. This most probably is due to the data gap before JD 91, which was caused by failure of the global radiation sensor. Oscillations in air temperature during summer and before Julian day 241 are not correlated with any change in NDVI, even if air temperature decreases below 10 °C. In contrast, small decreases in air temperature after JD 241 were associated with decreases in NDVI.

3.1.3. Daily variation in broadband NDVI

To provide a background for analysis of satellite-derived NDVI, daily variation in broadband NDVI was investigated. Results from typical clear, partly cloudy, and cloudy days from 1997 to 2001 are shown in Fig. 4. Clear days were selected such that sunshine hours occurred during more than 70% of the day length, while cloudy days indicate sunshine duration less than 30% of the time.

The daily variation in broadband NDVI is small on clear days. The mean absolute deviation for all clear days in 1997 was 2.4% of daily average NDVI, 1.7% for both 1999 and 2000, and 1.8% for 2001. The daily patterns were also similar, with relatively low values around noon and higher values in early morning and late afternoon. A slightly larger mean absolute deviation was found for partly cloudy days (4.2% in 1997, 3.0% in 1999, 4.5% in 2000, and 4.6% in 2001). Surprisingly, the daily pattern of broadband NDVI on partly cloudy and clear days was extremely similar. With increased length of cloud cover, daily patterns in broadband NDVI were more diverse. The mean absolute deviation increased to 9.7% in 1997, 11.1% in 1999, 12.5% in 2000, and 8.4% in 2001. Although broadband NDVI is little influenced by solar zenith angle and is stable on partly cloudy days, dense clouds obviously modify the spectral quality and reflectance of light in the wavelength bands utilized. Nevertheless, broadband NDVI seems a rather stable vegetation index as compared with satellite-derived NDVI.

Fig. 2. Annual course in broadband NDVI and daily average air temperature at Hyytiälä, Finland for 1997, 1999, and 2000.
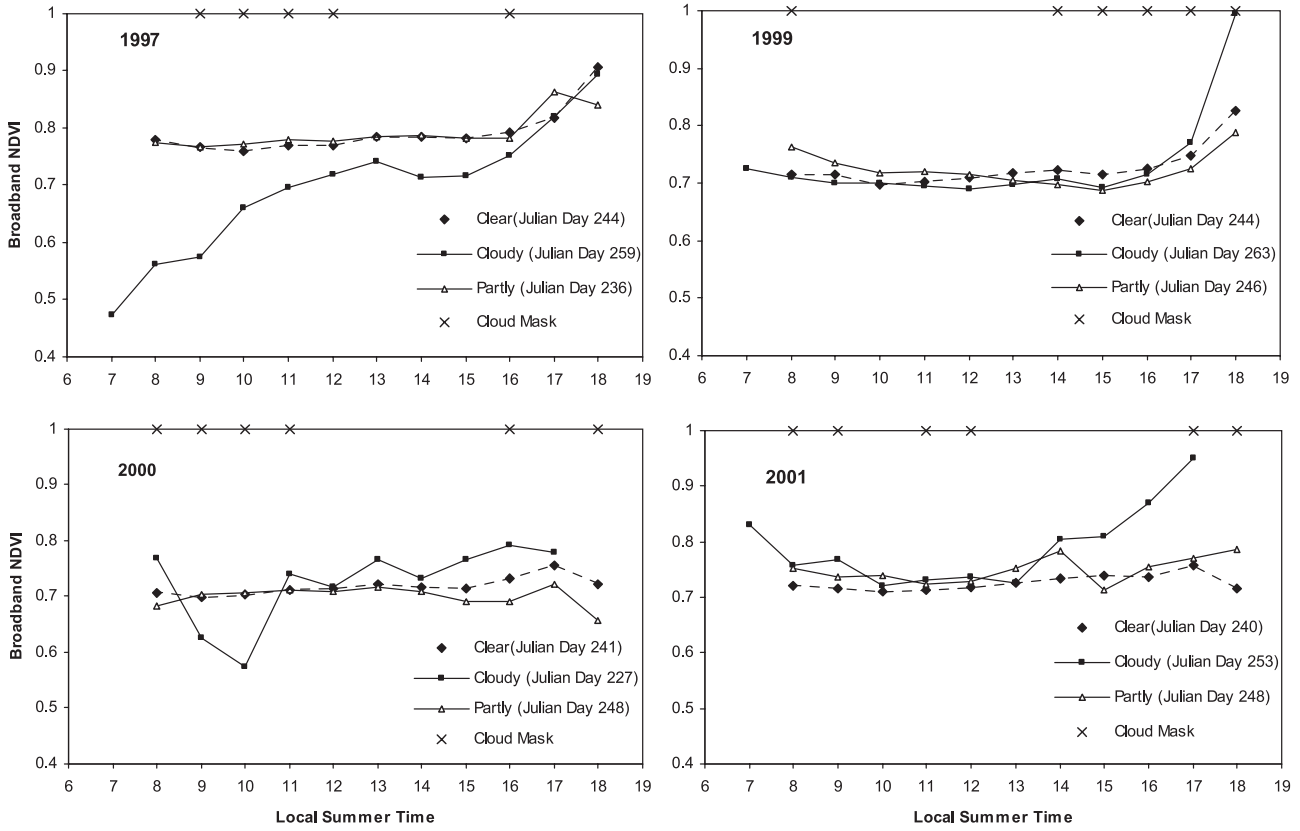
Fig. 4. Daily variation of broadband NDVI with clear, partly cloudy, and cloudy weather conditions in 1997, 1999, 2000, and 2001 at Hyytiälä, Finland.
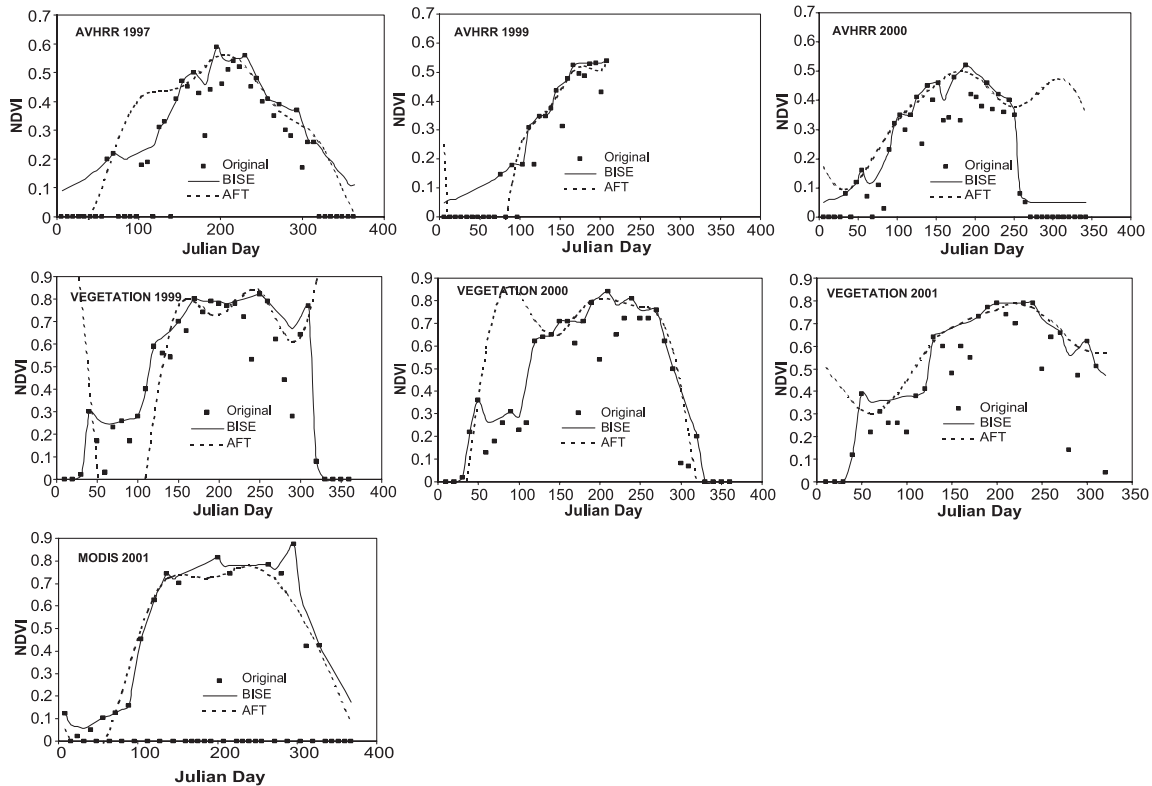

Fig. 5. Downloaded composite and smoothed NDVI times series from different satellite-borne sensors during various years for Hyytiäla, Finland.

Table 1
Regression comparison (R^2) of the satellite-derived NDVI from different smoothing methods as a function of broadband NDVI in various years in Hyytiälä, Finland

Data source	Smoothing method	1997		1999		2000		2001	
		All	GP	All	GP	All	GP	All	GP
AVHRR	FFT	0.42	0.7			0.35	0.58		
	BISE	0.43	0.82			0.09	0.13		
VEGETATION	FFT			0.01	0.67	0.14	0.1	0.52	0.8
	BISE			0.28	0.71	0.20	0.76	0.63	0.77
MODIS	FFT							0.44	0.89
	BISE							0.75	0.84

Results are given for the entire year and for Julian days 90–270 (growth period=GP).

3.2. Satellite-derived NDVI

3.2.1. Relationships between NDVIs from different sensors

The downloaded composited NDVI data (original from data source) from three satellite-borne sensors together with smoothed time series by the adjusted Fourier transform and BISE methods are illustrated in Fig. 5. All downloaded NDVI, independent of the specific data source, exhibited sudden decreases, which were obviously not caused by changes in the vegetation. Both the adjusted Fourier transform and BISE smoothed NDVIs followed the trends in original composite NDVI but showed less variation. However, the adjusted Fourier transform NDVI exhibited large deviations at the beginning and end of the year, while BISE smoothed NDVI remained consistent with the composite NDVI observations.

The relationships between the smoothed NDVI time series from different methods were examined by regression analysis. The regression coefficient ranged from 0.28 to 0.96 if all interpolated daily NDVI are included in the analysis. The regressions improve if only data from the summer growth period are used (from JD 90 to 270; with exceptions in year 2000 for VEGETATION NDVI and AVHRR NDVI).

Narrow band NDVI (satellite-derived NDVI) may have a different value from broadband NDVI; however, the seasonal patterns should correspond if both are similar indicators for changes in vegetation characteristics. Thus, we compared satellite-derived and broadband NDVI (Table 1). For AVHRR NDVI, adjusted Fourier transform was more consistent from year to year and exhibited a higher R^2 value except during 1997 and 1999 when BISE performed better. For VEGETATION NDVI, BISE performed better than the adjusted Fourier transform in all years. For MODIS NDVI, both methods produce a high quality NDVI time series during the growth period, but BISE had provided a higher R^2 value when the entire annual data set was used.

An effort to obtain phenological indices from smoothed satellite-derived NDVI time series based on the method of Reed et al. (1994) failed. None of the satellite-derived NDVI time series allowed estimation of the end-of-season at this site (Table 2). Although onset-of-greenness information was obtained from adjusted Fourier transform NDVI time series, the indicated dates were determined when average air temperature was below 0 °C. No onset-of-greenness points were distinguishable from BISE smoothed NDVI time series.

3.3. Applications of NDVI time series

3.3.1. Relationship of NDVI to GPP

GPP is an integrative expression of overall function of aboveground vegetation in assimilation of carbon. Since changes in the physiology and structure of plant canopies, i.e. development of pigment systems and leaf area, are directly viewed by NDVI, comparisons at flux tower locations such as Hyytiälä can provide useful insight into the coupling of phenology, ecosystem physiology, and remote sensing. Fig. 6

Table 2
Phenological information retrieved from smoothed satellite-derived NDVI time series in various years at Hyytiälä, Finland

Data source	Smoothing method	1997		1999		2000		2001	
		Onset-of-greenness	End-of-season	Onset-of-greenness	End-of-season	Onset-of-greenness	End-of-season	Onset-of-greenness	End-of-season
AVHRR	FFT	26 (−3.3 °C)	n	43 (−7.8 °C)	n	36 (−2.7 °C)	n		
	BISE	n	n	n	n	n	n		
VEGETATION	FFT			64 (−6.5 °C)	n	n	n	66	310
	BISE			n	n	n	n	n	n
MODIS	FFT							31	n
	BISE							26	n

Average daily temperature on indicated days is given in parentheses. n indicates that a determination was not possible.
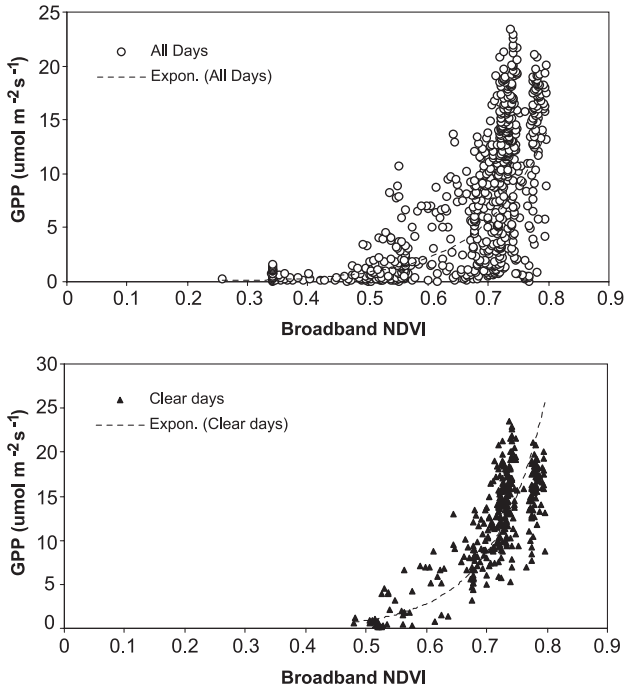
Fig. 6. Scatter diagrams of broadband NDVI and GPP for the Scots pine forest at Hyytiälä, Finland. The GPP data set includes daily integrated values from the years of 1997, 1999, and 2000.

Fig. 7. Relationship between FAPAR and broadband NDVI under clear weather conditions at Hyytiälä, Finland during the years of 1997, 1999, and 2000.

shows the scatter diagrams of broadband NDVI and GPP for all weather conditions and only clear weather conditions for the years of 1997, 1999, and 2000 when both broadband NDVI and GPP are available.

The curve fit to the data for all weather conditions is (GPP in μmol m^{-2} s^{-1}):

$$GPP = 0.0081e^{(9.34 * NDVI_{BB})} \left(R^2 = 0.50\right) \quad (9)$$

The R^2 is improved if only clear weather days are used in the analysis:

$$GPP = 0.0031e^{(11.33 * NDVI_{BB})} \left(R^2 = 0.72\right) \quad (10)$$

It is evident that the broadband NDVI tends to be saturated in relation to GPP at large NDVI values (>0.7). Nevertheless, with changes from spring to summer or from summer to fall, there is a strong correlation between NDVI and GPP despite small changes in LAI. Also, there seems to be interannual variability in the relationship, which is evident from the clustering of values at two NDVI maxima.
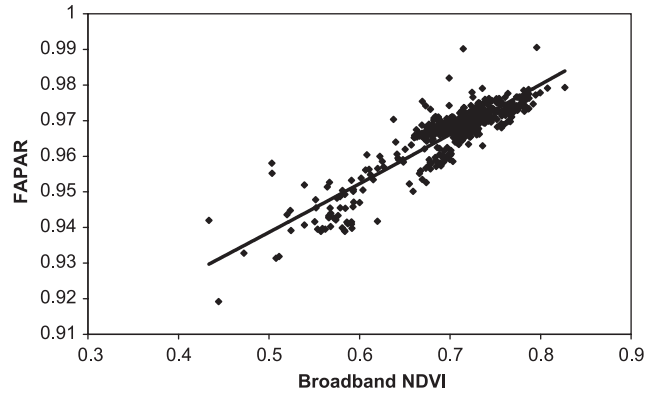
Since high NDVI and the saturation phenomenon usually occur on clear days with strong solar radiation in summer, we might speculate that good indications of seasonal controls on gas exchange may possibly be read from the data but when the maximum carbon uptake capacity of the canopy is achieved, other factors, e.g., temperature or water availability, strongly influence day to day in GPP and limit the information that is available from simple correlation analyses.

Utilizing smoothed satellite-derived NDVI time series, exponential relationships were similarly obtained (Table 3). In contrast to broadband NDVI, the smoothed satellite-derived data exhibited higher R^2 with all weather conditions included. Smoothing with BISE provided better results with R^2 values similar to those obtained with broadband NDVI.

3.3.2. Relationship with FAPAR

A linear relationship was obtained between FAPAR and broadband NDVI on clear days (Fig. 7):

$$FAPAR = 0.138 NDVI + 0.869 \left(R^2 = 0.79\right) \quad (11)$$

The R^2 decreased to 0.69 if all weather conditions were included:

$$FAPAR = 0.521 NDVI + 0.605 \left(R^2 = 0.69\right) \quad (12)$$

In the case of satellite-derived NDVI time series, a logistic relationship was obtained for FAPAR (Table 4). The

Table 3
Exponential relationships between GPP and smoothed satellite-borne NDVI time series and fitted parameters for model: GPP=$a*e^{b*NDVI}$ at Hyytiälä, Finland

Data source	Smoothing method	GPP							
		All				Clear days			
		a	b	R^2	n	a	b	R^2	n
AVHRR	FFT	0.107	9.917	0.67	505	0.472	7.087	0.37	204
	BISE	0.139	9.603	0.76	436	0.533	6.871	0.58	204
VEGETATION	FFT	0.821	2.991	0.41	346	1.589	2.637	0.22	299
	BISE	0.43	4.166	0.60	346	0.506	4.194	0.53	299

Table 4

Logistic relationships between FAPAR and smoothed satellite-derived NDVI time series and fitted parameters for model: FAPAR=$a+b$*ln(NDVI) in Hyytiälä, Finland

Data source	Smoothing method	FAPAR							
		All				Clear days			
		a	b	R^2	n	a	b	R^2	n
AVHRR	FFT	1.016	0.067	0.26	772	0.994	0.032	0.53	345
	BISE	0.995	0.043	0.15	772	0.986	0.021	0.48	345
VEGETATION	FFT	0.969	0.041	0.13	471	0.972	0.017	0.15	299
	BISE	0.969	0.031	0.12	471	0.978	0.035	0.54	299

correspondence between smoothed and FAPAR was low in all cases. For AVHRR NDVI, adjusted Fourier transformed NDVI had a stronger relationship with FAPAR than did BISE smoothed NDVI, while the opposite is true for VEGETATION NDVI.

4. Discussion and conclusions

The use of satellite-derived NDVI time series for describing phenological changes in vegetation at large scales has been demonstrated in a number of studies (e.g., Birky, 2001; Justice et al., 1985; Moody & Johnson, 2001). These analyses provide a basis for monitoring fluctuations and trends in surface characteristics as driven by interannual climate variability, climate change, and other natural and anthropogenic effects that impact the functioning of ecosystems. The derived phenological information has provided a basis for discriminating land cover and is widely applied in land cover classification (e.g., Loveland et al., 1991; DeFries and Townshed, 1994; Townshend et al., 1987).

Time series of NDVI have also been used to derive biophysical parameters critical to process models, FPAR and LAI in TURC (Ruimy et al., 1996); FPAR, soil water content, and evapotranspiration in GLO-PEM (Prince, 1991); FPAR in CASA (Potter et al., 1993) and LAI in BEPS (Liu et al., 1999). Nevertheless, the quality of NDVI time series after compositing either has been ignored or is not detailed in the these studies, leaving open the questions of how well a coupling between actual ecosystem responses and remote sensing of change has been achieved, and how specifically NDVI provides indication with respect to particular changes in ecosystem structure and function The satellite-derived NDVI time series decrease temporal resolution of observations depending on the compositing period. Moreover, the whiskbroom sensors (AVHRR, MODIS) alter the pixel size with scan angle by as much as a factor of 4 (Van Leeuwen et al., 1999). These limitations on temporal and spatial resolution of satellite-derived NDVI time series as well as remaining effects of clouds make direct comparisons with on-the-ground response difficult (Huemmrich et al., 1999). The strong effects of temporal sampling, remaining cloud cover, and data processing are apparent from the comparisons presented in Fig. 5 and Table

1. One possible way to increase temporal resolution to a daily time-step is to interpolate the smoothed NDVI time series by BISE or Fourier wave adjustment. However, the interpolation may lead to a large bias. Such bias is only revealed by comparison with ground-based NDVI time series. As shown in Table 1, only with recent data from MODIS was there a good correspondence between broadband and satellite-derived NDVI.

One of the reasons detailed ground-based NDVI time series are seldom produced is that most spectroradiometers used in remote sensing are not designed to operate automatically and to be exposed to the weather, which limits data collection. Micrometeorology based NDVI provides a new potential as a benchmark criterion in the validation and study of NDVI time series. Compared with satellite-derived data, micrometeorology-based NDVI is not affected by atmospheric conditions (Fig. 4). Thus, a ground-based network of NDVI estimates will provide a very powerful tool for evaluation of remote sensing NDVI estimates and associated corrections. Existing tower-based networks (e.g., FLUXNET, Baldocchi et al., 2001) provide anchor stations for such activities.

Moreover, one can use the broadband NDVI directly as input into models that simulate ecosystem function (e.g., GPP). This will allow us to evaluate the assumptions and algorithms of remote sensing-based GPP algorithms, eliminating the uncertainties that occur due to atmospheric effects. While it would be desirable to install high spectral resolution instruments at tower sites, the broadband NDVI is advantageous since most instrumentation is are already installed at many sites and the required extension may be economically achieved.

Any comparisons with remote-sensing based NDVI must of course recognize that the wavelengths used in broadband NDVI calculation are quite different from those used for satellite-derived NDVI. Nevertheless, similar relationships between ecosystem response and both broadband or satellite-borne NDVI should be expected, as shown by Huemmrich et al. (1999) who compared the broadband NDVI with narrowband NDVI from helicopter-mounted multiband modular radiometer (MMR) measurements over the BOREAS sites.

Broadband NDVI may be more closely related to canopy physiology than satellite-derived NDVI. It is less influenced by weather conditions and the temporal link to ecosystem

observations may be determined separately in individual investigations. Thus, broadband NDVI should provide the appropriate tool for identifying biophysical parameters for ecological models via reflective properties. Simultaneous examination of broadband and satellite-derived NDVI and comparison with ground-based information from ecosystem study sites must be emphasized in order to couple remote sensing with detailed knowledge of ecosystem process regulation, for example with GPP and carbon balances. In this way, the scatter shown in Figs. 6 and 7 may eventually be interpreted, and the empirical functions shown may be replaced with others based on ecosystem process understanding. As a goal, we may hope to obtain consistent relationships between NDVI and critical biophysical variables rather than the confounded results given in Figs. 6 and 7 together with Tables 3 and 4. Satellite-derived NDVI remains our only choice for generalization in large-scale investigations. Thus, intensified examination of the influences of smoothing and downscaling of satellite-derived NDVI is inevitable.

Acknowledgements

Appendix A

Adjusted Fourier transform details

There are missing data in the sequence of downloaded NDVI, since clouds may occur during the entire compositing period and the resulting values are eliminated by the "cloud mask". Moreover, some errors in NDVI still exit which produce a data sequence with sudden decreases and increases. Since further adjustment of the NDVI time series is necessary, we applied the AFT suggested by Sellers et al. (1994).

The adjusted Fourier transform of NDVI time series is based on two assumptions:

(1) NDVI time series should vary smoothly at any given point in time;
(2) External factors influencing NDVI and leading to errors can only decrease the value of NDVI.

Fourier series can be grouped as:

$$Y_i' = \sum_{j=1}^{m} a_j \cos\big((j-1)\varphi_i + b_j \sin((j-1)\varphi_i\big) \qquad (A1)$$

where a_j and b_j are Fourier coefficients, n the number of points in the sequence, and m is the number of harmonics.

As for weekly NDVI time series, $n=52$ and m is set to 7 in this study.

The modified robust least-squares optimizing technique from Sellers et al. (1994) has been applied. In this modification, the negative deviations receive low weights during fitting, while positive deviations obtain high weights based on the assumption that errors in the NDVI result in lower values. The procedures are:

(1) First insert 0 for all missing data before fitting of the Fourier series;
(2) The Fourier series are fitted through the data using the least-squares method.

$$\big([F]^T[F]\big)[c] = [F]^T[Y] \qquad (A2)$$

where $[Y]$ is the observed data, c the Fourier constants that must be solved for, and $[F]$ the values of $\cos((j-1)\phi_i)$ and $\sin((j-1)\phi_i)$ that correspond to the phase of data points y_i.
(3) The weights, W_i, are calculated according to distance from the fitted curve

$$W_i = 0, \quad if \ \ U_i \leq -k$$

$$W_i = (1 + (U_i + r)/k)^4, \quad if \ \ -k < U_i < -r$$

$$W_i = 1, \quad if \ \ -r \leq U_i \leq r$$

$$W_i = (1 + (U_i - r)/k)^2, \quad if \ \ U_i > r \qquad (A3)$$

with $U=(Y-Y')/M$, M the median of the absolute difference values of Y' and Y, $k=2$, $r=M/20$;
(4) Fourier series are fitted through the data with the weights W taken into account;
(5) Each point is checked against its original value and its four nearest neighbors. The new value is not to exceed the maximum of the five original values by more than 2% or to be lower than the original value.

References

Asrar, G., Myneni, R. B., & Choudhury, B. J. (1992). Spatial heterogeneity in vegetation canopies and remote sensing of absorbed photosynthetically active radiation: A modeling study. *Remote Sensing of Environment, 41*, 85–101.

Azzali, S., & Menenti, M. (1999). Mapping isogrowth zones on continental scale using temporal Fourier analysis of AVHRR-NDVI data. *JAG, 1*, 9–20.

Baldocchi, D., Falge, E., Gu, L., Olson, R., Hollinger, D., Running, S., et al. (2001). FLUXNET: A new tool to study the temporal and spatial variability of ecosystem-scale carbon dioxide, water vapor, and energy flux densities. *Bulletin of the American Meteorological Society, 82*, 2415–2434.

Birky, A. K. (2001). NDVI and a simple model of deciduous forest seasonal dynamics. *Ecological Modelling, 143*, 43–58.

Briggs, W. L., & Hensen, V. E. (1995). *The DFT: An owner's manual for the discrete Fourier transform*. Philadelphia, PA: Society for Industrial and Applied Mathematics.

Brown, J. F., Loveland, T. R., Merchant, J. W., Reed, B. C., & Ohlen, D. O. (1993). Using multisource data in global land-cover characterization: Concepts, requirements, and methods. *Photogrammetric Engineering and Remote Sensing*, 59, 977–987.

Choudhury, B. J. (1987). Relationships between vegetation indices, radiation absorption, and net photosynthesis evaluated by sensitivity analysis. *Remote Sensing of Environment*, 22, 209–233.

Cihlar, J., Manak, D., & Voisin, N. (1994). AVHRR bi-directional reflectance effects and compositing. *Remote Sensing of Environment*, 32, 427–437.

Deering, D. W., 1978. Rangeland reflectance characteristics measured by aircraft and spacecraft sensors. PhD Dissertation, Texas A&M University, College Station, TX. 338 pp.

DeFries, R. S., & Townshend, J. R. G. (1994). NDVI-derived land cover classification at global scales. *International Journal of Remote Sensing*, 15(17), 3567–3586.

Dijk, A., Callis, S. L., Sakamoto, C. M., & Decker, W. L. (1987). Smoothing index profiles: An alternative method for reducing radiometric disturbance in NOAA/AVHRR data. *Photogrammetric Engineering and Remote Sensing*, 53, 1059–1067.

Duchemin, B., Berthelot, B., Dedieu, G., Leroy, M., & Maisongrande, P. (2002). Normalisation of directional effects in 10-day global syntheses derived from VEGETATION/SPOT: II. Validation of an operational method on actual data sets. *Remote Sensing of Environment*, 81, 101–113.

Duchemin, B., Goubier, J., & Courrier, G. (1999). Monitoring phenological key stages and cycle duration of temperate deciduous forest ecosystems with NOAA/AVHRR data. *Remote Sensing of Environment*, 67, 68–82.

Duchemin, B., & Maisongrande, P. (2002). Normalisation of directional effects in 10-day global syntheses derived from VEGETATION/SPORT: I. Investigation of concepts based on simulation. *Remote Sensing of Environment*, 81, 90–100.

Eidenshink, J. C., & Faundeen, J. L. (1994). The 1 km AVHRR global land data set: First stages in implementation. *International Journal of Remote Sensing*, 15, 3443–3462.

Evans, D. L., Zhu, Z., & Winterberger, K. (1993). Mapping forest distributions with AVHRR data. *World Resource Review*, 5, 66–71.

Falge, E., Baldocchi, D. D., Tenhunen, J. D., et al. (2001). Gap filling strategies for defensible annual sums of net ecosystem exchange. *Agricultural and Forest Meteorology*, 107, 43–69.

Falge, E., Baldocchi, D. D., Tenhunen, J. D., Aubinet, M., Bakwin, P., Berbigier, P., et al. (2002). Seasonality of ecosystem respiration and gross primary production as derived from FLUXNET measurements. *Agricultural and Forest Meteorology*, 113, 53–74.

Falge, E., Tenhunen, J., Aubinet, M., Bernhofer, C., Clement, R., Granier, A., et al. (2003). A model-based study of carbon fluxes at ten European forest sites. In: R. Valentini (Ed.), *Fluxes of Carbon, Water and Energy of European Forests, Ecological Studies, vol. 163*, (pp. 151–177). Heidelberg: Springer Verlag.

Gamon, J. A., Field, C. B., Goulden, M. L., Griffin, K. L., Hartley, A. E., Joel, G., et al. (1995). Relationships between NDVI, canopy structure, and photosynthesis in three California vegetation types. *Ecological Applications*, 5, 28–41.

Goward, S. N., & Huemmrich, K. F. (1992). Vegetation canopy PAR absorptance and the normalized difference vegetation index: An assessment using the SAIL model. *Remote Sensing of Environment*, 39, 119–140.

Goward, S. N., Kerber, A., Dye, D. G., & Kalb, V. (1987). Comparison of North and South American biomes from AVHRR observations. *Geocarto*, 2, 27–40.

Goward, S. N., Tucker, C. J., & Dulaney, D. G. (1985). North American vegetation patterns observed with the NOAA-7 advanced very high resolution radiometer. *Vegetation*, 64, 3–14.

Gutman, G. G. (1991). Vegetation indices from AVHRR: An update and future prospects. *Remote Sensing of Environment*, 35, 121–136.

Hill, M., & Donald, G. E. (2003). Estimating spatio-temporal patterns of agricultural productivity in fragmented landscapes using AVHRR NDVI time-series. *Remote Sensing of Environment*, 84, 367–384.

Holben, B. N. (1986). Characterization of maximum value composites from temporal AVHRR data. *International Journal of Remote Sensing*, 7, 1417–1434.

Huemmrich, K. F., Black, T. A., Jarvis, P. G., McCaughey, J. H., & Halls, F. G. (1999). High temporal resolution NDVI phenology from micrometeorological radiation sensors. *Journal of Geophysical Research*, 104(D22), 27935–27944.

Huete, A., Justice, C., & van Leeuwen, W., (1999). MODIS Vegetation Index (MOD 13), Algorithm Theoretical Basis Document (Version 3).

James, M. E., & Kalluri, S. N. V. (1994). The pathfinder AVHRR land data set: An improved coarse resolution data set for terrestrial monitoring. *International Journal of Remote Sensing*, 15, 3347–3363.

Justice, C. O., Townshend, J. R. G., Holben, B. N., & Tucker, C. J. (1985). Analysis of the phenology of global vegetation using meteorological satellite data. *International Journal of Remote Sensing*, 6, 1271–1318.

Knyazikhin, Y., Glassy, J., Privette, J. L. Tian, Y., Lotsch, A., Zhang, Y., et al., (1999). MODIS Leaf Area Index (LAI) and Fraction of Photosynthetically Active Radiation Absorbed by Vegetation (FPAR) Product (MOD15) Algorithm Theoretical Basis Document. http://www.eospso.gsfc.nasa.gov/atbd/modistables.html.

Liu, J., Chen, J. M., Cihlar, J., & Chen, W. (1999). Net primary productivity distribution in the BOREAS region from a process model using satellite and surface data. *Journal of Geophysical Research*, 104, 27735–27754.

Loveland, T. R., Merchant, J. W., Ohlen, D. O., & Brown, J. F. (1991). Development of a land-cover characteristics database for the conterminous U.S. *Photogrammetric Engineering and Remote Sensing*, 57(11), 1453–1463.

Moody, A., & Johnson, D. M. (2001). Land-surface phonologies from AVHRR using the discrete Fourier transform. *Remote Sensing of Environment*, 75, 305–323.

Prince, S. D. (1991). A model of regional primary production for use with coarse resolution satellite data. *International Journal of Remote Sensing*, 12, 1313–1330.

Prince, S. D., & Tucker, C. J. (1986). Satellite remote sensing of rangelands in Botswana: II. NOAA AVHRR and herbaceous vegetation. *International Journal of Remote Sensing*, 7, 1555–1570.

Potter, C. S., Randerson, J. T., Field, C. B., Matson, P. A., Vitousek, P. M., Mooney, H. A., et al. (1993). Terrestrial ecosystem production—A process model based on global satellite and surface data. *Global Biogeochemical Cycles*, 7, 811–841.

Reed, B. C., Brown, J. F., VanderZee, D., Loveland, T. R., Merchant, J. W., & Ohlen, D. O. (1994). Measuring phenological variability from satellite imagery. *Journal of Vegetation Science*, 5, 703–714.

Ross, J., & Sulev, M. (2000). Sources of errors in measurements of PAR. *Agricultural and Forest Meteorology*, 100, 103–125.

Ruimy, A., Dedieu, G., & Saugier, B. (1996). TURC: A diagnostic model of continental gross primary productivity and net primary productivity. *Global Biogeochemical Cycles*, 10, 269–286.

Running, S. W., & Hunt, E. R. (1993). Generalization of a forest ecosystem process model for other biomes, BIOME-BGC, and an application for global scale models. In J. R. Ehleringer, & C. B. Field (Eds.), *Scaling physiological processes: Leaf to globe* (pp. 141–158). San Diego, CA: Academic.

Running, S. W., & Nemani, R. R. (1988). Relating seasonal patterns of the AVHRR vegetation index to simulated photosynthesis and transpiration of forest in different climates. *Remote Sensing of Environment*, 24, 347–367.

Sellers, P. J. (1987). Canopy reflectance, photosynthesis, and transpiration: II. The role of biophysics in the linearity of their interdependence. *Remote Sensing of Environment*, 21, 143–183.

Sellers, P. J., Tucker, C. J., Collatz, G. J., Los, S. O., Justice, C. O., Dazlich, D. A., et al. (1994). A global 1 by 1 NDVI data set for climate studies: Part 2. The generation of global fields of terrestrial biophysical

parameters from the NDVI. *International Journal of Remote Sensing*, *15*, 3519–3545.

Spanner, M. A., Pierce, L. L., Running, S. W., & Peterson, D. L. (1990). The seasonality of AVHRR data of temperate coniferous forests: Relationship with leaf area index. *Remote Sensing of Environment*, *33*, 97–112.

Tenhunen, J. D., Valentini, R., Köstner, B., Zimmermann, R., & Granier, A. (1998). Variation in forest gas exchange at landscape to continental scales. *Annales des Sciences Forestières*, *55*, 1–12.

Townshend, J. R. G., Justice, C. O., & Kalb, V. T. (1987). Characterization and classification of South American land cover types using satellite data. *International Journal of Remote Sensing*, *8*, 1189–1207.

Townshend, J. R. G., Justice, C. O., Skole, D. & et al. The 1 km resolution global data set: Needs of the International Geosphere Biospehere Programme. *International Journal of Remote Sensing*, *15*, 3417–3441.

Tucker, C. J., & Sellers, P. J. (1986). Satellite remote sensing of primary productivity. *International Journal of Remote Sensing*, *7*, 1395–1416.

Valentini, R. (Ed.) (2003). *Fluxes of Carbon, Water and Energy of European Forests, Ecological Studies*, *vol. 163*. Heidelberg: Springer Verlag.

van Leeuwen, W. J. D., Huete, A. R., & Laing, T. W. (1999). MODIS vegetation index compositing approach: A prototype with AVHRR data. *Remote Sensing of Environment*, *69*, 264–280.

Vesala, T., Haataja, J., Aalto, P., et al. (1998). Long-term field measurements of atmosphere-surface interactions in boreal forest combining forest ecology, micrometeorology, aerosol physics and atmospheric chemistry. *Trends in Heat, Mass & Momentum Transfer*, *4*, 17–35.

Viovy, N., Arino, O., & Belward, A. S. (1992). The best index slope extraction (BISE): A method for reducing noise in NDVI time-series. *International Journal of Remote Sensing*, *13*, 1585–1590.

Wang, Q., Tenhunen, J., Falge, E., Bernhofer, Ch., Granier, A., & Vesala, T. (2004). Simulation and scaling of temporal variation in gross primary production for coniferous and deciduous temperate forests. *Global Change Biology*, *10*, 37–51.

Wang, Q., Watanabe, M., Hayashi, S., & Murakami, S. (2003). Using NOAA AVHRR data to assess flood damage in China. *Environmental Monitoring and Assessment*, *82*, 119–148.

Wylie, B. K., Meyer, D. J., Tieszen, L. L., & Mannel, S. (2002). Satellite mapping of surface biophysical parameters at the biome scale over the North America grasslands: A case study. *Remote Sensing of Environment*, *79*, 266–278.